Journal of Power Sources 195 (2010) 1984–1991

Contents lists available at ScienceDirect

Journal of Power Sources

journal homepage: www.elsevier.com/locate/jpowsour

Synthesis and hydriding properties of $Li_2Mg(NH)_2$

Tippawan Markmaitree, Leon L. Shaw*

Department of Chemical, Materials and Biomolecular Engineering, University of Connecticut, Storrs, CT 06269, USA

ARTICLE INFO

Article history:
Received 30 July 2009
Received in revised form
18 September 2009
Accepted 30 September 2009
Available online 21 October 2009

Keywords:
Hydrogen storage materials
Li–Mg ternary imide
Kinetics
Hydrogenation

ABSTRACT

The phase pure $Li_2Mg(NH)_2$ has been synthesized via a dehydriding treatment of a ball milled $2LiNH_2 + MgH_2$ mixture. This phase pure $Li_2Mg(NH)_2$ has been utilized to investigate its hydriding kinetics at the temperature range 180–220 °C. It is found that the hydriding process of $Li_2Mg(NH)_2$ is very sluggish even though it has favorable thermodynamic properties for near the ambient temperature operation. Holding at 200 °C for 10 h only results in 3.75 wt.% H_2 uptake. The detailed kinetic analysis reveals that the hydriding process of $Li_2Mg(NH)_2$ is diffusion-controlled. Thus, this study unambiguously indicates that the future direction to enhance the hydriding kinetics of this promising hydrogen storage material system should be to minimize the diffusion distance and increase the diffusion rate.

1. Introduction

Many efforts have been made in searching for viable hydrogen storage materials based on the Li–Mg–N–H systems, including mixtures of $2LiNH_2 + MgH_2$ [1–7], $Mg(NH_2)_2 + 2LiH$ [4,8–10], $3Mg(NH_2)_2 + 8LiH$ [11–13], $Mg(NH_2)_2 + 4LiH$ [10,13–16], $Mg(NH_2)_2 + 3LiH$ or LiH [17], and $MgN_2 + 4Li_3N_2$ [16]. Among these Li–Mg–N–H systems, $2LiNH_2 + MgH_2$ and $Mg(NH_2)_2 + 2LiH$ have exhibited promising storage properties with the combination of a respectable theoretical storage capacity of 5.6 wt.% H_2 and a favorable dehydriding enthalpy. The latter is determined using the Van't Hoff equation to be 39.0 kJ mol^{-1} H_2 [3,18], 40.4 kJ mol^{-1} H_2 [7], or 41.6 kJ mol^{-1} H_2 [5]. This thermodynamic property allows the hydrogen plateau pressure higher than 1 bar at temperatures below 100 °C, thereby imparting the $2LiNH_2 + MgH_2$ and $Mg(NH_2)_2 + 2LiH$ systems the potential for on-board storage applications [2,3]. Indeed, it has been demonstrated experimentally that $2LiNH_2 + MgH_2$ has a reversible hydrogen storage capacity of 5.2 wt.% at 200 °C with a hydrogen pressure of 30 bar [3,4].

It is suggested that the dehydriding reaction of the $2LiNH_2 + MgH_2$ mixture proceeds as follows [1,2]:

$$2LiNH_2 + MgH_2 \rightarrow Li_2Mg(NH)_2 + 2H_2 \quad (1)$$

The hydriding process of Reaction (1), however, produces $Mg(NH_2)_2$ and LiH, as shown below.

$$Li_2Mg(NH)_2 + 2H_2 \leftrightarrow Mg(NH_2)_2 + 2LiH \quad (2)$$

The subsequent reversible reactions take place according to Reaction (2) and do not go back to $LiNH_2$ and MgH_2 [1–3,19]. Such reaction pathways are due to the fact that $Mg(NH_2)_2 + 2LiH$ is thermodynamically more stable than $2LiNH_2 + MgH_2$, as recently established by several workers [4,6]. Therefore, with the starting material of either $2LiNH_2 + MgH_2$ or $Mg(NH_2)_2 + 2LiH$, the overall reversible hydriding and dehydriding reactions can be expressed by Reaction (2).

Despites its favorable thermodynamic property and moderate reversible storage capacity, $Mg(NH_2)_2 + 2LiH$ appears to have kinetic barriers for fuel-cell vehicle applications. In particular, the hydriding kinetics of this system is considerably slower than its dehydriding kinetics [7,20]. Specifically, complete dehydrogenation takes place in 15–30 min at 200–220 °C [6,7,9,20,21], whereas complete hydrogenation at the same temperature requires 3–5 h [7,20]. Thus, the hydriding process can be a bottleneck for the application of the $Mg(NH_2)_2 + 2LiH$ system. However, the aforementioned studies [6,7,9,20,21] do not provide the detailed quantitative analysis of the hydriding kinetics. To the best of our knowledge, the detailed quantitative analysis of the hydriding kinetics of $Li_2Mg(NH)_2$ has not been conducted so far. Nor has the rate-limiting step of the hydriding process of $Li_2Mg(NH)_2$ be analyzed yet. However, there is no doubt that such detailed studies are necessary in order to provide guidelines for improving the hydriding kinetics of $Li_2Mg(NH)_2$ in the future.

In this study, we have investigated the hydriding properties of $Li_2Mg(NH)_2$, particularly its kinetics, and conducted the quantitative analysis of the rate-limiting step of the hydriding process of $Li_2Mg(NH)_2$. In order to provide unambiguous evidence for analysis, the starting powder should contain only one active phase, i.e., $Li_2Mg(NH)_2$ without the presence of other active phases such as

* Corresponding author. Tel.: +1 860 486 2592; fax: +1 860 486 4745.
E-mail address: leon.shaw@uconn.edu (L.L. Shaw).

0378-7753/$ – see front matter © 2009 Elsevier B.V. All rights reserved.
doi:10.1016/j.jpowsour.2009.09.067

$LiNH_2$ and $Mg(NH_2)_2$. Thus, $Li_2Mg(NH)_2$ is synthesized first in this study since $Li_2Mg(NH)_2$ is not commercially available. The synthesis condition, hydriding kinetics, rate-limiting step, and absorption pressure–composition isotherm of $Li_2Mg(NH)_2$ established from the present study are reported below.

2. Materials and methods

There are several ways to synthesize $Li_2Mg(NH)_2$, starting with either $2LiNH_2 + MgH_2$ [5,7,20,22] or $Mg(NH_2)_2 + 2LiH$ [1,17,18,23]. In this study, the $2LiNH_2 + MgH_2$ mixture was used as the starting material. The $LiNH_2$ powder of 95% purity and the MgH_2 powder of 95% purity were purchased from Fisher Scientific and Alfa Aesar, respectively, and were mixed in a 2-to-1.1 molar ratio before ball milling. The addition of the 10% excess MgH_2 than that required by Reaction (1) was to prevent the escape of NH_3 from the system during synthesis. High-energy ball milling was conducted using a modified Szegvari attritor that has been shown to be effective in preventing the formation of the dead zone and producing uniform milling products within the powder charge [24]. Furthermore, a previous study has demonstrated that the seal of the canister of the attritor is air-tight and there is no oxidation during ball milling [25]. The canister of the attritor and balls 6.4 mm in diameter were both made of stainless steels. The loading of balls and the powder mixtures to the canister was performed in a glove-box filled with ultrahigh purity argon that contains Ar 99.999%, $H_2O < 1$ ppm, $O_2 < 1$ ppm, $H_2 < 3$ ppm, $N_2 < 5$ ppm, and THC < 0.5 ppm (to be referred as an Ar of 99.999% purity hereafter). The ball-to-powder weight ratio was 60:1, the milling speed was 600 rpm, and the milling temperature was maintained at 20 °C, achieved by water cooling at a flowing rate of 770 ml min^{-1}. The milling was performed under an Ar atmosphere of 99.999% purity, and the milling time was 180 min.

The ball milled mixture was subsequently subjected to a dehydriding treatment to form $Li_2Mg(NH)_2$. The dehydriding treatment comprised a series of dehydriding steps using a commercial Sieverts'-type pressure–composition isotherm (PCI) unit (Advanced Materials Corporation, PA). In a typical dehydriding treatment, the ball milled mixture of approximately 500 mg was loaded into the pressure chamber of the PCI unit inside a glove-box filled with Ar of 99.999% purity. The loaded chamber was evacuated to 10^{-3} bar at room temperature before being inserted into the hot zone of a pre-heated cylindrical furnace. The temperature, pressure, and hydrogen content in the sample (wt.%) were immediately recorded (after 30 s delay) using a program based on the Lab View software during the entire dehydriding treatment. The first step of the dehydriding treatment entailed dehydriding the ball milled mixture under a previously evacuated condition (10^{-3} bar) at a desired temperature for a specified duration. The second step of the dehydriding treatment was to release the gas that was built up inside the closed PCI chamber during the first step of the dehydriding treatment. This second step of the dehydriding treatment consisted of a series of repeated sub-steps (either 50 or 100 sub-steps) each of which contained holding for 15 min and then evacuation at the constant temperature. A total of three different dehydriding treatment conditions were investigated and are summarized in Table 1.

The as-synthesized $Li_2Mg(NH)_2$ phase was then investigated for its hydriding kinetics at 180, 200, and 220 °C with the starting H_2 pressure of 65 bar using the same PCI unit as that used for synthesizing $Li_2Mg(NH)_2$. After sample loading and pressurization at room temperature, the sample chamber was inserted into the hot zone of a pre-heated cylindrical furnace. The hydrogen uptake behavior was immediately recorded (after 30 s delay) as a function of the holding time using the Lab View software. The pressure–composition isotherm of the $Li_2Mg(NH)_2$ phase at 220 °C was also studied. The absorption PCI curve was taken with the pressure range from 0.03 to 95 bar and the equilibrium condition for each point, specified by the rate of pressure change, being smaller than 0.001 bar min^{-1}.

All the samples were analyzed using X-ray diffraction (XRD) to provide phase identification. The operation conditions for the XRD data collection were Cu Kα radiation, 40 kV, 40 mA, 2° min^{-1}, and 0.02°/step using a D5005 ADVANCE diffractometer. To prevent oxidation during XRD data collection, the sample was sealed in a capillary quartz tube and the loading of the sample to the tube was performed in a glove-box filled with Ar of 99.999% purity. The capillary quartz tube had a wall of 0.01 mm thick and thus was transparent to the X-ray beam. In many XRD analyses, 10 wt.% Si powder was added to the powder mixture as an internal standard for calibration of the peak position.

Many samples were also subjected to characterization using Fourier transform infrared spectroscopy (FTIR). The FTIR spectra were collected on a Niclotet Magna 560 FTIR spectrometer (resolution 4 cm^{-1}) using the potassium bromide (KBr) pellet method. The mixture of the sample (around 5 wt.%) and powdered KBr was ground using a mortar and pestle in the glove-box filled with Ar of 99.999% purity. The ground mixture was then transferred to a pellet press holder and pressed at 13 ksi to form a pellet 12 mm in diameter and approximately 0.5 mm in thickness. The sample pellets were briefly exposed to the air during hydraulic pressing and transferred to a compartment of the spectrometer. Prior to the collection of each spectrum, the background of air was measured and subtracted from the sample.

The specific surface area (SSA) of the powder before and after isothermal hydriding reactions was determined through nitrogen adsorption at 77K based on the Brunauer–Emmett–Teller (BET) method using a gas sorption analyzer (NOVA 1000, QUANTACHROME Corporation, FL). The loading of the sample (~0.05 g) into a sample cell with a Teflon stem filler was performed in a glove-box filled with Ar of 99.999% purity. The measurement was performed immediately after the sample was loaded in the instrument. The relative pressure (P/P_o) was 0.05 to 0.3 and the reported SSA data were calculated based on 5 points BET method [26].

3. Results and discussion

3.1. Synthesis of $Li_2Mg(NH)_2$

Fig. 1a shows the pressure rise during the first step of the dehydriding treatment of the ball milled $2LiNH_2 + MgH_2$ mixture at 210 °C (condition #1 in Table 1). The corresponding H_2 released computed from the pressure rise and the volume of the closed chamber per sample weight percent is shown in Fig. 1b. It can be seen that the pressure rise is very fast at the beginning of the

Table 1
Summary of the dehydriding treatment conditions for synthesizing $Li_2Mg(NH)_2$.

ID of the dehydriding treatment	First-step dehydriding conditions	Second-step dehydriding conditions
Dehydriding condition #1	210 °C for 33-h holding in a previously evacuated chamber	210 °C for 12.5 h with 50 holding/evacuation sub-steps
Dehydriding condition #2	210 °C for 45-h holding in a previously evacuated chamber	210 °C for 25 h with 100 holding/evacuation sub-steps
Dehydriding condition #3	240 °C for 45-h holding in a previously evacuated chamber	240 °C for 25 h with 100 holding/evacuation sub-steps

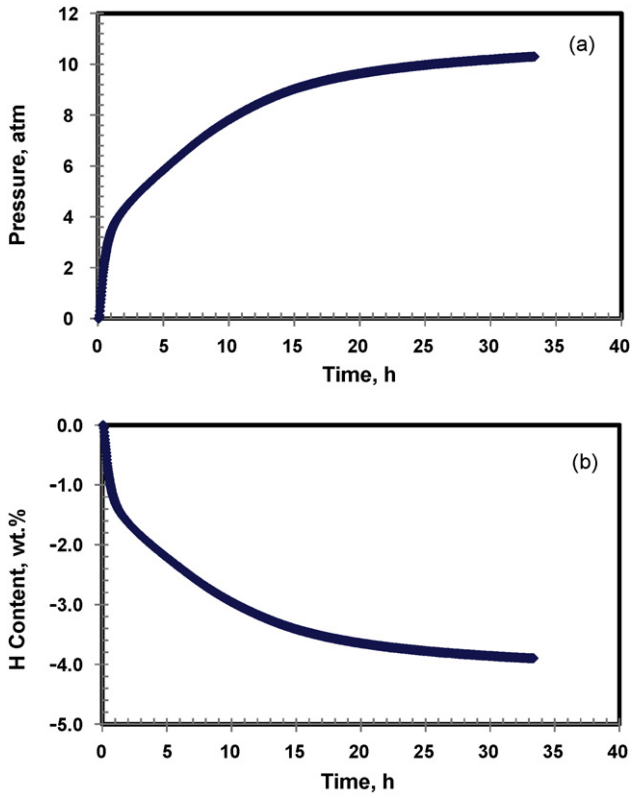

Fig. 1. The desorption profile of the $2LiNH_2 + MgH_2$ mixture at 210 °C in a closed PCI chamber under a previously evacuated condition: (a) shows the pressure rise in the closed chamber as a function of the holding time, and (b) shows the corresponding quantity of the hydrogen released as a function of the holding time.

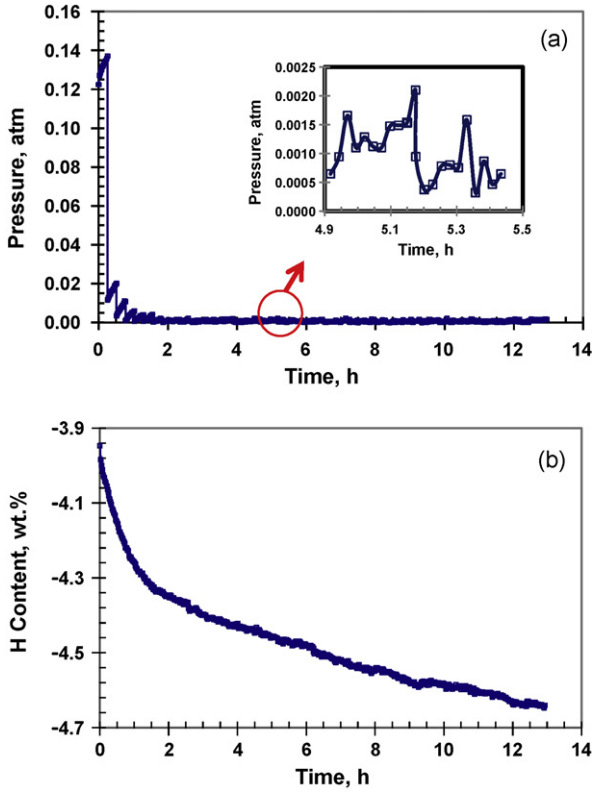

Fig. 2. The release profile of the $2LiNH_2 + MgH_2$ mixture in the second step of the dehydriding treatment at 210 °C with 50 holding/evacuation sub-steps: (a) shows the change of the pressure within the chamber as a function of the holding time and release sub-steps, and (b) shows the corresponding quantity of the hydrogen released as a function of the holding time and release sub-steps. The insert in (a) shows the detail of the pressure change in the 20th and 21st holding/evacuation sub-steps.

isothermal holding and becomes very slow near the end of the 33-h holding. The purpose of the prolonged holding time (33 h) was to provide sufficient time to allow MgH_2 to react with NH_3 because our previous study [27] has established that the formation of $Li_2Mg(NH)_2$ based on Reaction (1) is NH_3 mediated. Furthermore, the reaction between MgH_2 and the NH_3 derived from the decomposition of $LiNH_2$ is very slow [27,28]. Thus, to prevent emission of NH_3 during the dehydriding treatment, a prolonged holding is necessary. At the end of the 33-h holding the amount of H_2 released is 4.0 wt.% (Fig. 1b) if one assumes that there is no NH_3 inside the chamber. This amount of hydrogen is substantially lower than the theoretical 5.6 wt.% of Reaction (1). However, when the presence of the 10% excess MgH_2 and 10 wt.% impurities is considered, the theoretical storage capacity becomes 4.81 wt.% H_2. This value is still higher than 4.0 wt.% H_2 observed, suggesting that Reaction (1) has not completed yet in the 33-h holding at 210 °C.

In order to increase the dehydriding rate after the 33-h holding, the second step of the dehydriding treatment was to release the hydrogen gas from the PCI chamber to further drive the reaction between MgH_2 and $LiNH_2$ to completion. This was accomplished in about 13 h with 50 holding/evacuation sub-steps at 210 °C, as illustrated in Fig. 2a. The PCI chamber was closed for 15 min between every two consecutive evacuation sub-steps in order to allow MgH_2 to react with NH_3, if any, and to quantify how much hydrogen was released in the next evacuation step. As shown in Fig. 2a, the pressure of the PCI chamber increases gradually during each 15-min holding because of the continuous reaction between the remaining MgH_2 and $LiNH_2$ to produce $Li_2Mg(NH)_2$ and H_2. However, the pressure build-up becomes smaller as the number of the evacuation increases. At the end of the 50th holding sub-step the pressure within the PCI chamber is less than 0.003 bar (Fig. 2a). These 50 holding/evacuation sub-steps at 210 °C have released 0.64 wt.% H_2 (Fig. 2b), leading to a total amount of 4.64 wt% H_2 released in the dehydriding treatment.

The released 4.64 wt.% H_2, however, is still lower than the expected value of 4.81 wt.% H_2, suggesting an incomplete dehydriding reaction under the dehydriding condition #1 (Table 1). This is confirmed by the XRD analysis. As shown in Fig. 3, ball milling at 20 °C does not induce any chemical reactions or phase transformation, but results in finer crystallite sizes and/or the introduction of structural defects, as evidenced by the broadening of the XRD peaks after ball milling. The XRD pattern of the product from the dehydriding condition #1 exhibits a mixture of several phases, namely $LiNH_2$, MgH_2, and $Li_2Mg(NH)_2$. The $Li_2Mg(NH)_2$ peaks found in the dehydriding product are identical to those reported in Refs. [4,5].

Based on the result from the dehydriding condition #1, a second dehydriding condition (condition #2 in Table 1) was investigated. This dehydriding treatment entailed subjecting the ball milled $2LiNH_2 + MgH_2$ mixture to the first step of the dehydriding treatment at 210 °C for a 45-h holding in a closed PCI chamber, followed by the second step of the dehydriding treatment to release hydrogen at 210 °C for 25 h in 100 holding/evacuation sub-steps. Given the longer period of time in both the first and second steps of the dehydriding treatment under the dehydriding condition #2, it is expected that the dehydriding reaction can be closer to the completion. This is indeed the case, as evidenced by the XRD pattern of the product from the dehydriding condition #2 showing the lower intensities of the $LiNH_2$ (35.597°) and MgH_2 (35.744°) peaks around 35.7° (Fig. 3d) than those from the dehydriding condition #1 (Fig. 3c).

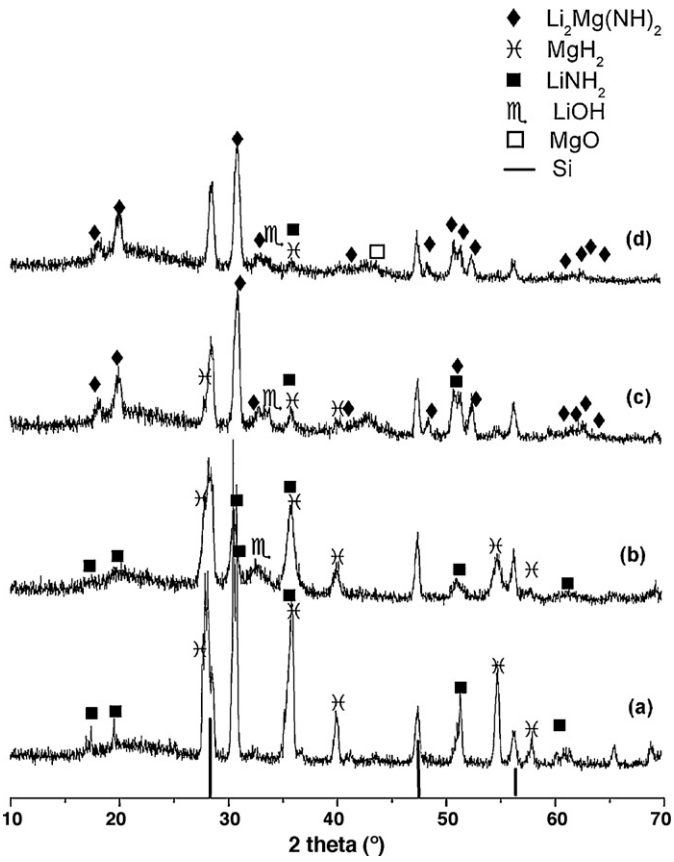

Fig. 3. XRD patterns of the $2LiNH_2 + MgH_2$ mixture with the addition of 10 wt.% Si powder: (a) without ball milling, (b) with ball milling at room temperature for 180 min, (c) after the dehydriding condition #1, and (d) after the dehydriding condition #2.

Fig. 3, however, cannot tell whether the peak around 35.7° is due to the incomplete reaction between MgH_2 and $LiNH_2$ or due to the presence of the 10% excess MgH_2 added. Therefore, a third dehydriding treatment (condition #3 in Table 1) was investigated. This comprised the first step of the dehydriding treatment at 240 °C for a 45-h holding, followed by the second step of the dehydriding treatment to release hydrogen at the same temperature for 25 h in 100 holding/evacuation sub-steps. The XRD pattern of the product from the dehydriding condition #3 is shown in Fig. 4. Note that no Si internal standard was added to these samples during the XRD data collection in order to reveal the strongest peak of MgH_2 at 27.947°; otherwise, this MgH_2 peak is overlapped with the strongest peak of the Si powder at 28.443° (see Fig. 3). It is clear from Fig. 4 that the intensities of MgH_2 peaks at 27.947° and 35.744° from the dehydriding condition #3 are lower than those from the dehydriding condition #2. Since there are no Mg peaks in any of these XRD patterns, it can be concluded that there is remaining MgH_2 in the dehydriding condition #2 due to the incomplete reaction between MgH_2 and $LiNH_2$. The tiny MgH_2 peaks at 27.947° and 35.744° in the dehydriding condition #3, however, are due to the 10% excess MgH_2 added.

In order to corroborate the conclusions above, the FTIR analysis was performed to characterize amide ($-NH_2$) and imide (–NH) structures. As shown in Fig. 5, the FTIR spectrum of the product from the dehydriding condition #3 results in two convoluted peaks, at 3183 and 3164 cm^{-1}, suggesting the formation of the –NH structure where–NH is bonded to a mixture of Li and Mg ions [23]. Furthermore, there are no bands from–NH_2 structure at 3313 and 3259 cm^{-1}, suggesting that $LiNH_2$ is completely consumed [4,23]. Therefore, it can be concluded that $2LiNH_2$ and MgH_2 have completely reacted to form $Li_2Mg(NH)_2$ except the 10% excess MgH_2 under the dehydring condition #3. Thus, the product from the dehydriding condition #3 is used for the following kinetic and thermodynamic analyses, discussed in Sections 3.2 and 3.3.

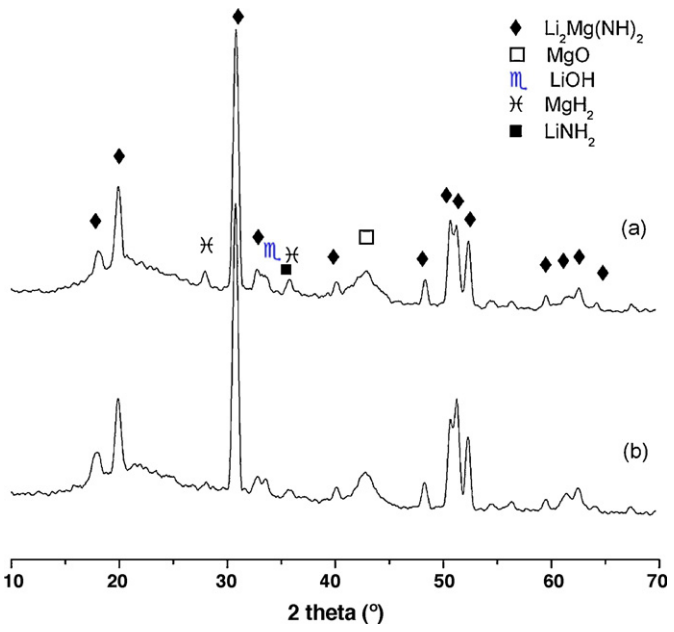

Fig. 4. XRD patterns of the $2LiNH_2 + MgH_2$ mixture without the addition of Si powder: (a) after the dehydriding condition #2 and (b) after the dehydriding condition #3.

3.2. The hydriding kinetics and rate-limiting step of $Li_2Mg(NH)_2$

Fig. 6 shows the isothermal hydriding kinetics of $Li_2Mg(NH)_2$ at three different temperatures (180, 200, and 220 °C) with the initial H_2 pressure of 65 bar. It is clear that the rates of hydrogen uptake for all the temperatures within the first 15 min are relatively fast with 28%, 23%, and 15% of the theoretical storage capacity for 220, 200, and 180 °C, respectively. Here, the theoretical storage capacity (4.81 wt.% H_2) is based on Reaction (2) after excluding the presence of the 10% impurities and 10% excess MgH_2 in the sample. The hydrogen uptake rate for 220 °C starts to slow down significantly after 15 min, and then levels off after 40 min. In contrast, the hydrogen uptake for 180 and 200 °C continues to increase but with a slightly slower rate than the initial 15 min. The total amounts of hydrogen uptake within 60 min at 180 and 200 °C are 1.36 and

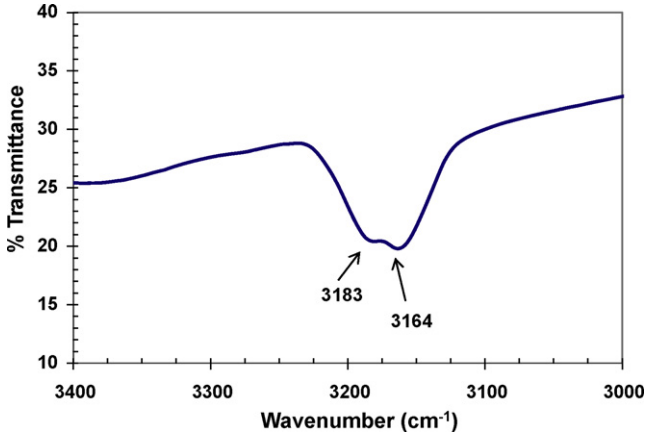

Fig. 5. FTIR spectrum of the $2LiNH_2 + MgH_2$ mixture after the dehydriding condition #3.

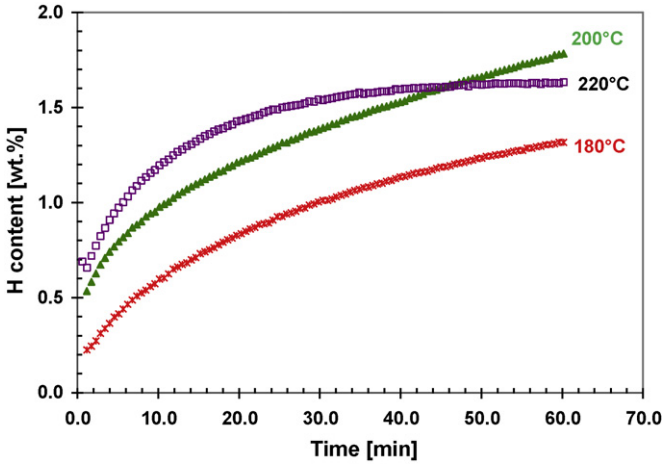

Fig. 6. The isothermal absorption curves of the phase pure $Li_2Mg(NH)_2$ at 180, 200, and 220 °C within a closed chamber with an initial hydrogen pressure of 65 bar.

1.78 wt.% or 28% and 37% of the theoretical storage capacity, respectively. Interestingly, the total amount of hydrogen uptake within 60 min at 220 °C is only 1.63 wt.%, less than the amount at 200 °C. This outcome is unexpected because increasing the temperature typically leads to an increased reaction kinetics. The reason for this unusual behavior is discussed in Section 3.3.

In order to identify the rate-limiting step for the hydriding process of $Li_2Mg(NH)_2$, the fraction of H_2 absorbed, f, as a function of the holding time, t, of each isothermal absorption curve in Fig. 6 have been analyzed using a shrinking core model [29–31]. With the use of this model, it assumes implicitly that Reaction (2) takes place via the growth of a shell of the LiH and $Mg(NH_2)_2$ mixture into the $Li_2Mg(NH)_2$ core during the hydriding process. The suitability of this model will be discussed in Section 3.3. Here, we will proceed with the analysis first. In this analysis, several possible rate-limiting steps have been considered, which include: (i) diffusion of a diffusing species through the product layer, (ii) movement of the reactant/product interface at a constant speed, (iii) nucleation and growth of the product, and (iv) adsorption of the gaseous phase at the surface of the solid particle. The corresponding equations for these rate-limiting steps have been derived previously [29–31] and are listed below, respectively.

$$(1-f)^{1/3} = 1 - \frac{{k_1}^{1/2}}{r}t^{1/2} \quad (3)$$

$$(1-f)^{1/3} = 1 - \frac{k_2}{r}t \quad (4)$$

$$f = 1 - \exp(-k_3 t^m) \quad (5)$$

$$f = k_4 r^2 t \quad (6)$$

here r is the average radius of $Li_2Mg(NH)_2$ particles, k_1, k_2, k_3 and k_4 are rate constants, and m is the mechanism constant, which varies from 1 to 4 depending on the detail of nucleation and growth of the products. To evaluate the hydriding kinetics at 180 and 200 °C shown in Fig. 6, Eqs. (3)–(6) need to be modified to take into account the incomplete uptake of H_2 at the end of each isothermal hydriding curve. For example, Eq. (3) should be modified to be [31]

$$(1-f'f)^{1/3} = 1 - \frac{{k_1}^{1/2}}{r}t^{1/2} \quad (7)$$

where f' is the fraction of H_2 absorbed at the end of the hydriding curve (within 60 min) in reference to the hydrogen storage capacity of the system, which is 4.81 wt.% H_2 as discussed previously. Thus, $f = 1$ at the end of the hydriding process, whereas $f' = 1$ only if the H_2 absorbed at the end of the hydriding segment equals the hydrogen storage capacity of the system (i.e., 4.81 wt.%). Otherwise, f' is smaller than 1. Similarly, Eqs. (4)–(6) should be modified, respectively, to be Eqs. (8)–(10):

$$(1-f'f)^{1/3} = 1 - \frac{k_2}{r}t \quad (8)$$

$$f'f = 1 - \exp(-k_3 t^m) \quad (9)$$

$$f'f = k_4 r^2 t \quad (10)$$

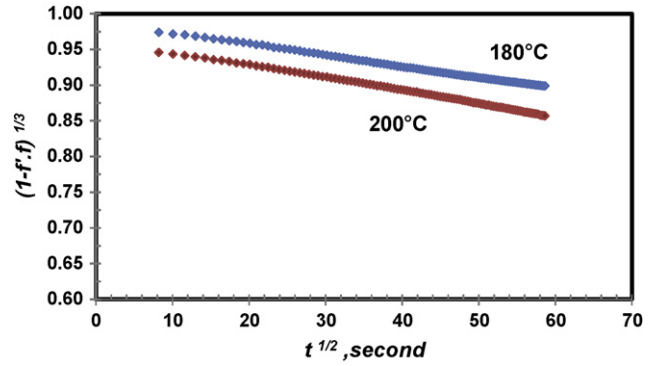

Fig. 7. The amounts of H_2 absorbed by $Li_2Mg(NH)_2$ at 180 and 200 °C shown in Fig. 6 are plotted in $(1-f'f)^{1/3}$ vs $t^{1/2}$, as defined by Eq. (7).

Fig. 7 shows the analyses of the hydriding curves of 180 and 200 °C in Fig. 6 with the aid of Eq. (7). The curve fitting of the hydriding data presented in Fig. 7 through the least-squares method results in the following two linear equations:

$$(1-f'f)^{1/3} = 0.989 - 0.0016t^{1/2} \quad \text{with } R^2 = 0.999 \text{ for } T = 180\ ^\circ\text{C} \quad (11)$$

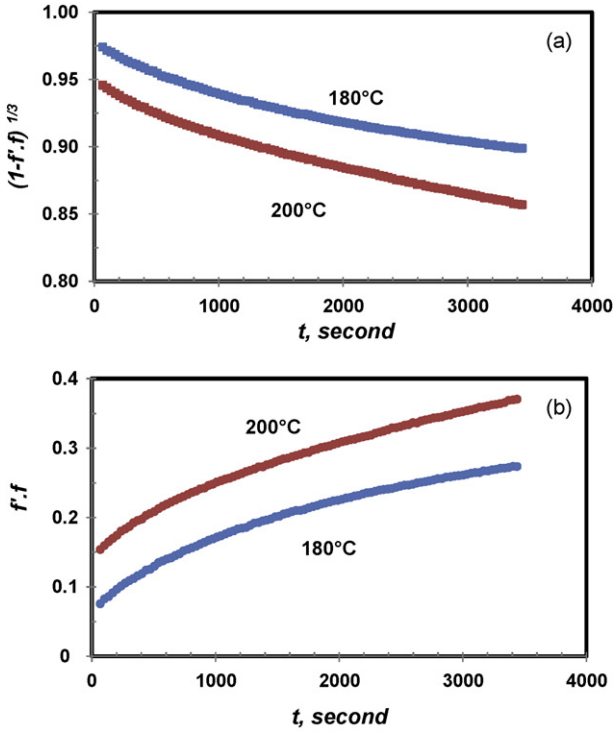

Fig. 8. (a) The amounts of H_2 absorbed by $Li_2Mg(NH)_2$ at 180 and 200 °C shown in Fig. 6 are plotted in $(1-f'f)^{1/3}$ vs t, as defined by Eq. (8), and (b) plotted in $f'f$ vs t, as described by Eq. (10).

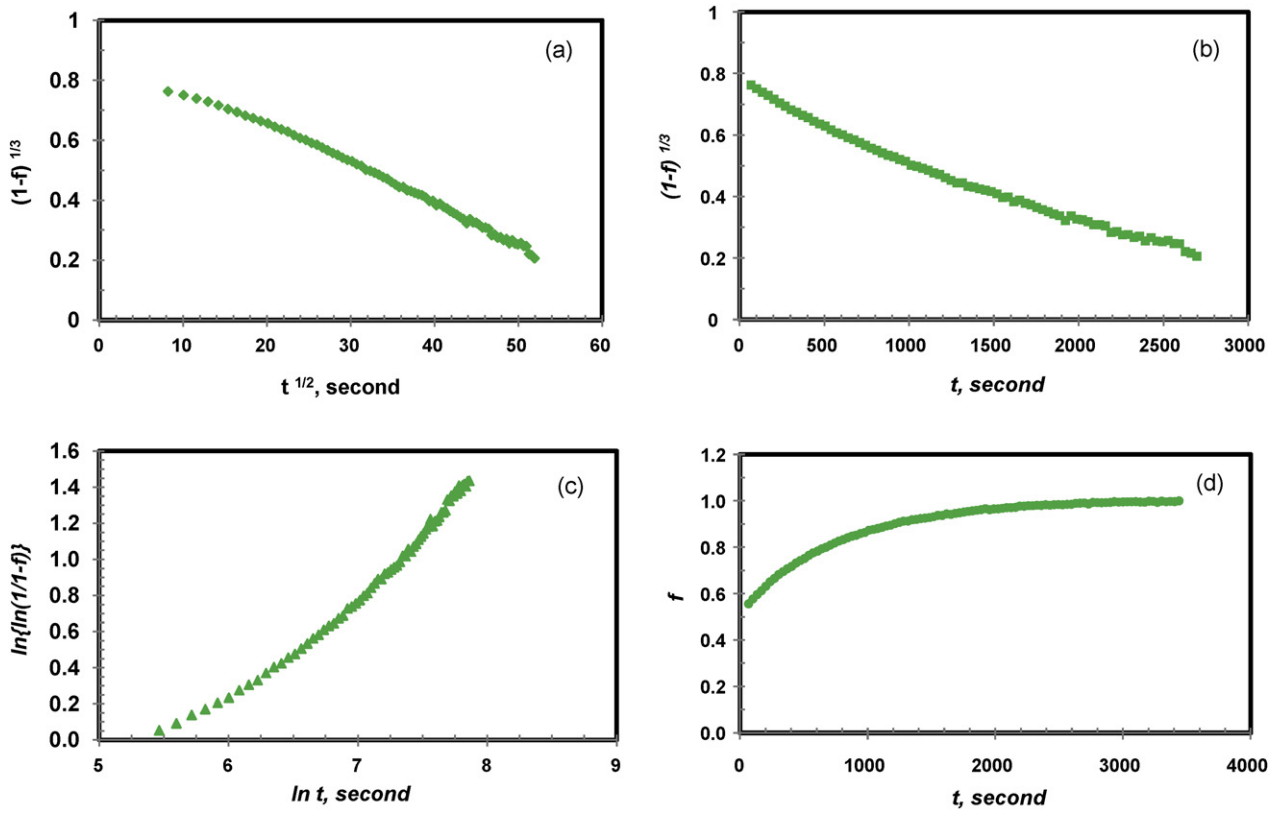

Fig. 9. Analysis of the hydriding curve at 220 °C shown in Fig. 6 with the aid of (a) Eq. (3) for the diffusion-controlled reaction, (b) Eq. (4) for the moving-interface-controlled reaction, (c) Eq. (5) by plotting $\ln\{\ln(1/1-f)\}$ vs $\ln t$ for the nucleation-and-growth-controlled reaction, and (d) Eq. (6) for the adsorption-controlled reaction.

$$(1-f'f)^{1/3} = 0.965 - 0.0018t^{1/2} \quad \text{with } R^2 = 0.998 \text{ for } T = 200\ ^\circ\text{C} \tag{12}$$

It is very clear that the hydriding data of $Li_2Mg(NH)_2$ at 180 and 200 °C fit well with the diffusion-controlled reaction. On the contrary, the hydriding data do not fit the other models. For example, the analyses of the moving-interface-controlled reaction based on Eq. (8) and the adsorption-controlled reaction based on Eq. (10) are shown in Fig. 8. The linear equations obtained via curve fitting through the least-square method for the moving-interface-controlled reaction are

$$(1-f'f)^{1/3} = 0.963 - 0.00002t \quad \text{with } R^2 = 0.962 \text{ for } T = 180\ ^\circ\text{C} \tag{13}$$

$$(1-f'f)^{1/3} = 0.936 - 0.00002t \quad \text{with } R^2 = 0.980 \text{ for } T = 200\ ^\circ\text{C} \tag{14}$$

and the corresponding equations for the adsorption-controlled reaction are

$$f'f = 0.108 + 0.00005t \quad \text{with } R^2 = 0.954 \text{ for } T = 180\ ^\circ\text{C} \tag{15}$$

$$f'f = 0.183 + 0.00006t \quad \text{with } R^2 = 0.972 \text{ for } T = 200\ ^\circ\text{C} \tag{16}$$

Clearly, these curve fittings do not result in satisfactory results. First of all, their *R*-squared values are not as good as those for the diffusion-controlled reaction. Second, the first constant on the right hand side of the equation from the diffusion-controlled reaction is close to 1, whereas that constant for the moving-interface-controlled reaction is not as close to 1 as the diffusion-controlled reaction. To have a physical meaning, this constant should be equal to 1. The larger departure from 1 for the moving-interface-controlled reaction, in conjunction with its unsatisfactory *R*-squared value, indicates that this mechanism is not the rate-limiting step. Similar reasoning can be applied to exclude the adsorption-controlled reaction and the nucleation-and-growth-controlled reaction (not shown here) as the rate-limiting step. Therefore, the diffusion-controlled reaction can best describe the hydriding reaction of $Li_2Mg(NH)_2$ at 180 and 200 °C.

In the case of the hydriding process at 220 °C, the amount of the absorbed H_2 has already reached the limit of the hydriding reaction at the H_2 pressure of 65 bar. This statement will be justified in Section 3.3. Here, it suffices to say that the kinetic models for such a hydriding process should contain no modified factor, *f'*, because of the completion of the reaction. Therefore, Eqs. (3)–(6) are used in the analysis. Fig. 9 shows the analyses of the hydriding data at 220 °C with the aid of Eqs. (3)–(6). The linear equations obtained from curve fitting through the least-square method for the diffusion-controlled reaction, moving-interface-controlled reaction, and adsorption-controlled reaction are shown below, respectively.

$$(1-f'f)^{1/3} = 0.989 - 0.0016t^{1/2} \quad \text{with } R^2 = 0.989 \tag{17}$$

$$(1-f'f)^{1/3} = 0.709 - 0.0002t \quad \text{with } R^2 = 0.979 \tag{18}$$

$$f'f = 0.722 - 0.0001t^{1/2} \quad \text{with } R^2 = 0.783 \tag{19}$$

Indisputably, the diffusion-controlled reaction provides the best fit for the dehydriding data at 220 °C. The same conclusion applies when the nucleation-and-growth-controlled reaction (Fig. 9c) is compared with the diffusion-controlled reaction. Therefore, the hydriding process of $Li_2Mg(NH)_2$ at 180, 200, and 200 °C can all be well described as the diffusion-controlled reaction.

3.3. The pressure–composition isotherm of $Li_2Mg(NH)_2$

In order to understand the unusual hydrogen absorption behavior of $Li_2Mg(NH)_2$ at 220 °C (Fig. 6), the absorption pressure–composition isotherm of the $Li_2Mg(NH)_2$ phase was conducted at 220 °C, as shown in Fig. 10. The data obtained by Luo and Sickafoose [4] is included for comparison. It is noted that the isotherm exhibits two plateaus, as discovered by Luo and Sickafoose [4]. Furthermore, it is very obvious that the $Li_2Mg(NH)_2$ from this study has a higher plateau pressure than the $Li_2Mg(NH)_2$ investigated by Luo and Sickafoose [4]. Specifically, the equilibrium pressure reported by Luo and Sickafoose is ~54 bar, whereas the $Li_2Mg(NH)_2$ from this study has an equilibrium pressure at 95 bar, about 40 bar higher than that reported by Luo and Sickfoose. It is noted that other studies [3,7,17,18] also report the equilibrium pressure similar to the value by Luo and Sickafoose [4].

It is well known that the equilibrium pressure (P_{eq}) in the PCI is related to the reaction enthalpy (ΔH) and entropy (ΔS) by the Van't Hoff equation [32]:

$$\ln(P_{eq}) = -\frac{\Delta H}{RT} + \frac{\Delta S}{R} \quad (20)$$

where R is the gas constant and T is the temperature. Based on the plateau pressure as a function of temperature, the dehydriding enthalpy has been determined with the aid of Eq. (20) to be 39.0 kJ mol^{-1} H_2 [3,18], 40.4 kJ mol^{-1} H_2 [7], and 41.6 kJ mol^{-1} H_2 [5]. Taking the dehydriding enthalpy as 39 kJ mol^{-1} H_2 by Luo and Ronnebro [3] and the equilibrium pressure of 54 bar at 220 °C by Luo and Sickafoose [4], the dehydriding entropy can be found with the aid of Eq. (20) to be 112 J mol K^{-1} H_2. This value is similar to the experimental value reported by Yang et al. [5]. Assuming that ΔS remains to be 112 J mol K^{-1} H_2 and taking the equilibrium pressure as 90 bar at 220 °C (Fig. 10), the dehydriding enthalpy in this study is estimated to be 36.5 kJ mol^{-1} H_2 with the aid of Eq. (20). Thus, the higher plateau pressure found in this study can be attributed to the reduced enthalpy of $Li_2Mg(NH)_2$, the increased enthalpy of $2LiH + Mg(NH_2)_2$, or both.

One interesting and scientifically important question is why the $Li_2Mg(NH)_2$ phase in this study has a reduced enthalpy or the $2LiH + Mg(NH_2)_2$ mixture has an increased enthalpy when compared with other studies [3,4,7,17,18]. The answer to this important question undoubtedly requires extensive studies. At this stage, we tentatively propose that different sample preparation methods have resulted in the increased plateau pressure observed in this study. It is noted that the samples in other studies [3,4,7,17,18] are all prepared using SPEX mills, whereas the samples in this study are processed using an attritor. A SPEX mill provides predominantly normal impact to the powder mixture, whereas an attritor offers a good combination of normal impact and shear deformation to the powder mixture. Thus, ball milling using an attritor is likely to provide a higher degree of mechanical activation to the $2LiNH_2 + MgH_2$ mixture than that using a SPEX mill. Another potential source for the unusually high plateau pressure is the way the $Li_2Mg(NH)_2$ is made in this study, which comprises holding $Li_2Mg(NH)_2$ at 240 °C for 70 h with 100 holding/evacuation cycles (condition #3 in Table 1). Such a long-time holding at 240 °C with 100 holding/evacuation cycles can potentially lower the defect concentration in the crystalline $Li_2Mg(NH)_2$ and thus its enthalpy. However, which factor really contributes to the unusually high plateau pressure is outside the scope of this study. Future works are clearly needed to clarify this. Finally, it should be mentioned that the unusually high plateau pressure is not due to the presence of a small amount of MgO in the sample because the presence of MgO has been reported before with no observations of the unusually high plateau pressure [7,17].

According to Fig. 10, the equilibrium hydrogen content at 220 °C for a hydrogen pressure of 65 bar is approximately 1.5 wt.% which is close to the value observed in Fig. 6, indicating that the hydrogen uptake at 220 °C lower than that at 200 °C during isothermal holding is due to the exhaustion of the thermodynamic driving force at 220 °C. In contrast, the isothermal hydrogenation at 180 and 200 °C shown in Fig. 6 is not limited by the thermodynamic driving force. Therefore, kinetic modeling using Eqs. (3)–(6) for 220 °C and Eqs. (7)–(10) for 180 and 200 °C is very appropriate.

It should be mentioned that the two plateaus in the pressure–composition isotherm have been proposed to correspond to the following reactions [4]:

$$Li_2Mg(NH)_2 + 0.6H_2 \leftrightarrow Li_2MgN_2H_{3.2} \quad (0 < wt.\%H_2 < 1.5) \quad (21)$$

$$Li_2MgN_2H_{3.2} + 1.4H_2 \leftrightarrow Mg(NH_2)_2 + 2LiH \quad (1.5 < wt.\%H_2 < 5.1) \quad (22)$$

Thus, the diffusion-controlled reaction identified in Fig. 6 is mainly for the first-stage reaction shown by Eq. (21) since the maximum hydrogen uptake for all the three conditions in Fig. 6 is near 1.5 wt.% H_2. In order to find out the rate-limiting step for the second-stage reaction shown by Eq. (22), isothermal hydriding at 200 °C for a longer holding time has been conducted and is shown in Fig. 11. With the longer holding time the maximum hydrogen uptake is 3.75 wt.%, well into the second-stage reaction. The kinetic modeling using Eqs. (7)–(10) unambiguously indicates

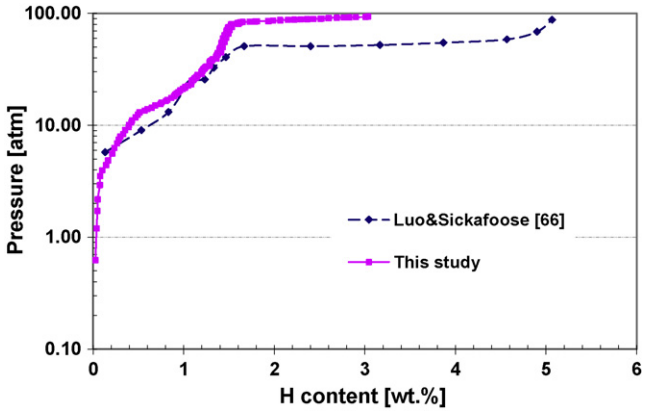

Fig. 10. The absorption pressure–composition isotherm of $Li_2Mg(NH)_2$ at 220 °C. The data obtained by Luo and Sickafoose [4] is included for comparison. The measurement of the PCI is terminated at 95 bar because it has reached the instrument capability.

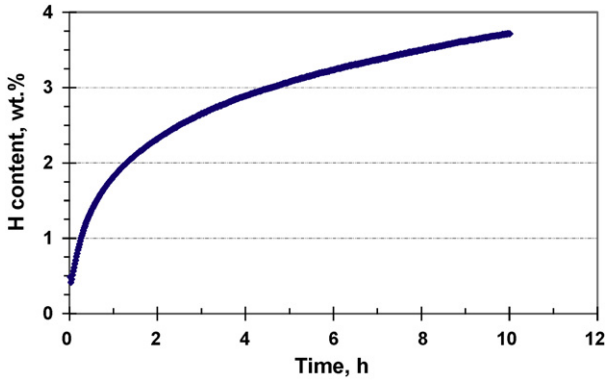

Fig. 11. The isothermal absorption curve of the phase pure $Li_2Mg(NH)_2$ at 200 °C within a closed chamber with an initial hydrogen pressure of 68 bar.

that the rate-limiting step for the isothermal hydriding process shown in Fig. 11 is diffusion-controlled. Therefore, it is concluded that even the second-stage reaction shown by Eq. (22) is diffusion-controlled. In addition, it should be emphasized that the present kinetic analysis only reveals that diffusion is the rate-limiting step for the hydriding process of $Li_2Mg(NH)_2$. Whether hydrogenation proceeds with one or multiple elementary steps cannot be derived from this kinetic analysis. However, by combining the results from Luo and Sickafoose [4], it can be concluded that both stage reactions are diffusion-controlled.

The specific surface area of the sample before isothermal hydriding at 200 °C shown in Fig. 11 has been measured and is found to be 34.18 $m^2\,g^{-1}$. This value decreases to 22.99 $m^2\,g^{-1}$ after isothermal hydriding at 200 °C for 10 h. There are two implications with the measured change in the SSA. First, it suggests that particle sizes have grown during this 10-h hydriding process. This is consistent with the expectation of long-term thermal exposure at 200 °C. Second, it suggests that there is no particle cracking during this 10-h hydriding process; otherwise, the SSA would have increased. Therefore, this result justifies the use of the shrinking core model to identify the rate-limiting step and to analyze the hydriding kinetics of $Li_2Mg(NH)_2$. If particle cracking takes place during the hydriding process, the shrinking core model would not be suitable for analysis because H_2 can have the access to and react with the inner $Li_2Mg(NH)_2$ through macro- or micro-cracks in the $Li_2Mg(NH)_2$ particle. Therefore, the conclusion of the diffusion-controlled hydriding reaction derived from the shrinking core model also suggests that there is no particle cracking during the hydriding process, which is in good agreement with the measurements of the SSA before and after 10 h hydriding.

Finally, it should be pointed out that the present kinetics analysis is based on the assumption of monodisperse particles. In the real systems like the one here, some degrees of spread in particle sizes are present. Thus, strictly speaking, the effect of particle size distribution should be included in the analysis. Nevertheless, the effect of particle size distribution (e.g., Gaussian distribution or log-normal distribution) on hydriding and dehydriding kinetics has been investigated previously [33]. It is concluded that the effect of particle size distribution is negligible when the fraction reacted, f, is lower than 60%. However, the deviation from the behavior of monodisperse particles becomes noticeable, but no more than 5%, when f is higher than 60% [33]. Thus, the monodisperse particle model should provide good approximation for the real system investigated here.

4. Concluding remarks

In this study the phase pure $Li_2Mg(NH)_2$ has been synthesized via a dehydriding treatment of a ball milled $2LiNH_2 + MgH_2$ mixture. It is found that the reaction between $LiNH_2$ and MgH_2 to form $Li_2Mg(NH)_2$ is very slow during the dehydriding treatment. A total of 70 h at 240 °C with multiple evacuation sub-steps is required to achieve the complete conversion from $2LiNH_2 + MgH_2$ to $Li_2Mg(NH)_2$, while the same holding time at 210 °C with the same number of the evacuation sub-steps does not lead to the completion of the reaction. The isothermal hydriding kinetics of the phase pure $Li_2Mg(NH)_2$ have been evaluated at 180, 200 and 220 °C. It is found that the hydriding process of $Li_2Mg(NH)_2$ is also very sluggish even though it has favorable thermodynamic properties for near the ambient temperature operation. Holding at 200 °C for 10 h only results in 3.75 wt.% H_2 uptake. This clearly is not adequate for on-board storage applications. The detailed kinetic analysis reveals that the rate-limiting step for the hydriding process of $Li_2Mg(NH)_2$ is diffusion. Thus, this study unequivocally indicates that the future direction to enhance the hydriding kinetics of this promising hydrogen storage material system should entail: (i) nano-engineering to minimize the diffusion distance, (ii) high-energy ball milling to introduce lattice defects and thus increase the diffusion coefficient, and/or (iii) doping to increase the lattice distortion and thus the diffusion rate. The $Li_2Mg(NH)_2$ in this study exhibits higher plateau pressure than the counterpart investigated by other researchers. It appears that this is due to different processing conditions used to synthesize $Li_2Mg(NH)_2$. However, the precise cause for the higher plateau pressure remains to be investigated in the future.

Acknowledgements

This work was supported under the U.S. Department of Energy (DOE) Contract No. DE-FC36-05GO15008. The vision and support of Dr. Ned T. Stetson, DOE Technology Manager, are greatly appreciated.

References

[1] Z. Xiong, G. Wu, J. Hu, P. Chen, Adv. Mater. 16 (2004) 1522–1525.
[2] W. Luo, J. Alloys Compd. 381 (2004) 284–287.
[3] W. Luo, E. Rönnebro, J. Alloys Compd. 404–406 (2005) 392.
[4] W. Luo, S. Sickafoose, J. Alloys Compd. 407 (2006) 274.
[5] J. Yang, A. Sudik, C. Wolverton, J. Alloys Compd. 430 (2007) 334–338.
[6] R. Janot, J.-B. Eymery, J.-M. Tarascon, J. Power Sources 164 (2007) 496–502.
[7] S. Barison, F. Agresti, S.L. Russo, A. Maddalena, P. Palade, G. Principi, G. Torzo, J. Alloys Compd. 459 (2008) 343–347.
[8] T. Ichikawa, N. Hanada, S. Isobe, H. Leng, H. Fujii, Mater. Trans. 46 (2005) 1–14.
[9] Y. Chen, C.-Z. Wu, P. Wang, H.-M. Cheng, Int. J. Hydrogen Energy 31 (2006) 1236–1240.
[10] M. Aoki, T. Noritake, G. Kitahara, Y. Nakamori, S. Towata, S. Orimo, J. Alloys Compd. 428 (2007) 307.
[11] H.Y. Leng, T. Ichikawa, T.S. Isobe, S. Hino, N. Hanada, H. Fujii, J. Alloys Compd. 404–406 (2005) 443–447.
[12] H.Y. Leng, T. Ichikawa, S. Hino, N. Hanada, S. Isobe, H. Fujii, J. Phys. Chem. B 108 (2004) 8763–8765.
[13] H.Y. Leng, T. Ichikawa, S. Hino, T. Nakagawa, H. Fujii, J. Phys. Chem. B 109 (21) (2005) 10744–10748.
[14] Y. Nakamori, G. Kitahara, K. Miwa, N. Ohba, T. Noritake, S. Towata, S. Orimo, J. Alloys Compd. 404–406 (2005) 396–398.
[15] Y. Nakamori, G. Kitahara, S. Orimo, J. Power Sources 138 (2004) 309–312.
[16] Y. Nakamori, G. Kitahara, K. Miwa, S. Towata, S. Orimo, Appl. Phys. A 80 (2004) 1–3.
[17] Z. Xiong, G. Wu, J. Hu, P. Chen, W. Luo, J. Wang, J. Alloys Compd. 417 (2006) 190.
[18] Z. Xiong, J. Hu, G. Wu, P. Chen, W. Luo, K. Gross, J. Wang, J. Alloys Compd. 398 (2005) 235–239.
[19] H.Y. Leng, T. Ichikawa, H. Fujii, J. Phys. Chem. B 110 (2006) 12964–12968.
[20] W. Luo, J. Wang, K. Stewart, M. Clift, K. Gross, J. Alloys Compd. 446–447 (2007) 336–341.
[21] Y. Chen, P. Wang, C. Liu, H.M. Cheng, Int. J. Hydrogen Energy 32 (2007) 1262–1268.
[22] A. Sudik, J. Yang, D. Halloday, C. Wolverton, J. Phys. Chem. C 111 (2007) 6568–6573.
[23] W. Lohstroh, M. Fichtner, J. Alloys Compd. 446–447 (2007) 332–335.
[24] Z.-G. Yang, L. Shaw, Nanostruct. Mater. 7 (8) (1996) 873–886.
[25] R. Ren, A.L. Ortiz, T. Markmaitree, W. Osborn, L. Shaw, J. Phys. Chem. B 110 (2006) 10567–10575.
[26] S. Brunauer, P.H. Emmett, E. Teller, J. Am. Chem. Soc. 60 (1938) 309–319.
[27] T. Markmaitree, W. Osborn, L. Shaw, Int. J. Hydrogen Energy 33 (2008) 3915–3924.
[28] T. Markmaitree, W. Osborn, L. Shaw, J. Power Sources 180 (2008) 535–538.
[29] T. Markmaitree, R. Ren, L. Shaw, J. Phys. Chem. B 110 (41) (2006) 20710–20718.
[30] L. Shaw, W. Osborn, T. Markmaitree, X. Wan, J. Power Sources 177 (2008) 500–505.
[31] X. Wan, T. Markmaitree, W. Osborn, L. Shaw, J. Phys. Chem. C 112 (2008) 18232–18243.
[32] L. Schlapbach, A. Zuttel, Nature 414 (2001) 353–358.
[33] M.H. Mintz, Y. Zeiri, J. Alloys Compd. 216 (1994) 159–175.